Available online at www.sciencedirect.com
ScienceDirect
Journal of Volcanology and Geothermal Research 165 (2007) 142 – 162
Journal of volcanology and geothermal research
www.elsevier.com/locate/jvolgeores

Variable regimes in magma systems documented in plagioclase zoning patterns: El Misti stratovolcano and Andahua monogenetic cones

Philipp Ruprecht *, Gerhard Wörner

GZG, Abt. Geochemie, Universität Göttingen, Goldschmidtstr. 1, 37077 Göttingen, Germany

Received 7 November 2006; received in revised form 5 June 2007; accepted 5 June 2007
Available online 12 June 2007

Abstract

Magmas may experience closed- or open-system evolution during their ascent and evolution in the upper crust. Chemically closed-system processes can involve heat transfer from underplating mafic magmas or decompression due to magma ascent. On the other hand, newly injected magmas can mix with the residing magma and hybridize. Plagioclase zonation patterns and electron microprobe major and trace element analysis constrain these contrasting scenarios for andesites from the 80 km^3 El Misti stratovolcano (5822 m) and a field of relatively small monogenetic Andahua scoria cones, both in southern Peru. In particular, Fe concentration in plagioclase reveals valuable information within a magmatic system to explore the dominance of closed- vs. open-system processes. Large and correlated Anorthite-Fe contrasts at resorption zones identify compositional mixing related to recharge. Subhorizontal An–Fe variations record thermal or water-induced effects. El Misti volcano, a large but still relatively youthful stratovolcano, is dominated during most of its approx. 120 ka history by closed-system effects during its evolution. Recharge and mixing mostly occurred cryptically as it is not recorded in drastic compositional changes in magmas or their phenocrysts.

A small volume erupted at El Misti, however, is affected by strong open-system behaviour as reflected in strongly correlated variations in An and Fe contents of plagioclase compositions. Its crystal population is texturally and chemically very similar to lavas of the monogenetic cinder cones of the Andahua Volcanic Field.

For the El Misti magma reservoir, resorption events caused by thermal effects or magma ascent are more frequent in comparison to the actual eruption frequencies. Many cycles of closed-system evolution (heat transfer and decompression) therefore occurred without resulting in an eruption.

Plagioclase zonations from lavas of the monogenetic Andahua field indicate that any mafic batch that intruded the much smaller reservoirs immediately triggered an eruption. By contrast, a large magma system that feeds El Misti volcano can easily accommodate a new batch without causing eruption.

Keywords: plagioclase zonation; magma chamber dynamics; continental arc magmatism; stratovolcano; monogenetic cinder cone field; El Misti; Andes, Peru

* Corresponding author. Present address: Department of Earth and Space Sciences, University of Washington, Box 351310, Seattle, WA 98195, USA. Tel.: +1 206 685 1910; fax: +1 206 543 0489.

E-mail addresses: ruprecht@u.washington.edu (P. Ruprecht), gwoerner@gwdg.de (G. Wörner).

0377-0273/$ - see front matter
doi:10.1016/j.jvolgeores.2007.06.002

1. Introduction

A prominent recorder of processes in magmatic systems prior to eruption is provided by the size, composition and in particular the chemical and isotopic zonation of phenocrysts (Davidson and Tepley, 1997). Fractional crystallisation, magma replenishment and wall-rock assimilation are the major processes of magma evolution. These affect temperature and composition within the storage system and result in a variable environment where processes such as convection, resorption and crystal growth may be effective at the same time. Plagioclase phenocrysts provide a core-to-rim geochemical record that reflects such progressive changes in the magma from which they grew.

A systematic view of the principal processes operating in magmatic systems beneath stratovolcanoes as derived from mineral zonations has not yet been fully developed. Information has been gathered mostly from individual case studies (e.g. Singer et al., 1995; Knesel et al., 1999; Ginibre et al., 2002a; Tomiya and Takahashi, 2005; Wallace and Bergantz, 2005; Triebold et al., 2006); and systematic patterns that would allow generalised conclusions are not observed. In this paper, a mineral zonation study on two South Peruvian volcanic centers in the Central Andean Volcanic Zone (CVZ, Fig. 1) has been carried out: El Misti stratovolcano (5822 m; 16°18′S, 71°24′W) and the Andahua monogenetic volcanic field (AVF; 15°32′S, 72°19′W). El Misti volcano and the AVF are both located at the volcanic front of the Recent volcanic chain of the Central Volcanic Zone of the Andes. El Misti is well suited for such a study because its stratigraphy is well known (Thouret et al., 2001) and volcanic rocks are all plagioclase-phyric.

Our approach follows that of Ginibre et al. (2002a,b) in applying backscattered electron (BSE) imaging techniques and quantitative trace element measurements on the scale of textural features by electron microprobe. Using BSE images enables us to directly correlate elemental compositions with textural features that may be related to varying pressure and temperature conditions. Compositional changes are recorded by trace element measurements. Open-system effects such as contamination and recharge by chemically distinct magma batches can be distinguished from changes in temperature, H_2O, and total pressure. Thus, we can distinguish between (a) physico-chemical processes of magma mixing with distinct chemistries, (b) chemically closed-system processes such as heating by new magma batches or decompression due to magma ascent, and (c) cryptic open-system behaviour. Such cryptic mixing is characterized by mixing of chemically similar magmas (Humphreys et al., 2006). Such information about magmatic processes from zonation patterns and geochemical information on trace elements from plagioclase phenocrysts provide important constraints on the understanding, reconstruction and modelling of the pre-eruptive evolution of El Misti and other comparable volcanic systems.

This approach also allows us to investigate the role of magma recharge and subsequent mixing as a trigger mechanism for volcanic eruption. We assess the question of how frequently volcanic eruptions occur in comparison to magma mixing events at the large El Misti volcano and the Andahua Volcanic Field. El Misti has a volume of ca. 80 km^3. After Thouret et al. (2001) and results from field work performed by the authors, El Misti's eruptive history covers the last 112 kyrs. Thus, assuming an average eruption volume a linear eruption rate approximation of about one event in every 200 years can be obtained. The lava flow field at Andahua consists of monogenetic scoria cones and lava flows, its total erupted volume is about 15 km^3 and eruption ages range from Upper Pleistocene to historic times (Delacour et al., 2007). By comparing the Andahua Volcanic Field with El Misti volcano we are also able to discern how new inputs affect small short-lived magmatic systems compared to large-evolved ones. Thus, this enables us to develop a better understanding of the relationship between processes and rates of magma mixing, magma system recharge and volcanic eruptions.

2. Setting

The past and future eruptive behaviour of El Misti volcano is of particular interest since it is located only 20 km northeast of Arequipa (2414 m), the second largest city in Peru (Fig. 1). El Misti's volcanic activity is characterized by alternations of effusive and explosive eruptions as well as avalanche deposits (Thouret et al., 2001). El Misti's last major eruption occurred three hundred years ago (Thouret et al., 2001). Recent and historic eruptions as well as fumarolic activity indicate that the magma system is active and new volcanic events may occur at any time. Besides the primary volcanic hazard directly from El Misti, landslides and lahars threaten the city of Arequipa due to channelling through the Rio Chili Canyon located in between the Nevado de Chachani to the northwest and El Misti volcano.

The Andahua Volcanic Field is a Holocene to historic scoria and lava field extending over an area of about 50 km × 30 km ENE of the Nevados de Coropuna complex of stratovolcanoes (Fig. 1, Delacour et al., 2007). The field is situated inside the Andahua Valley.

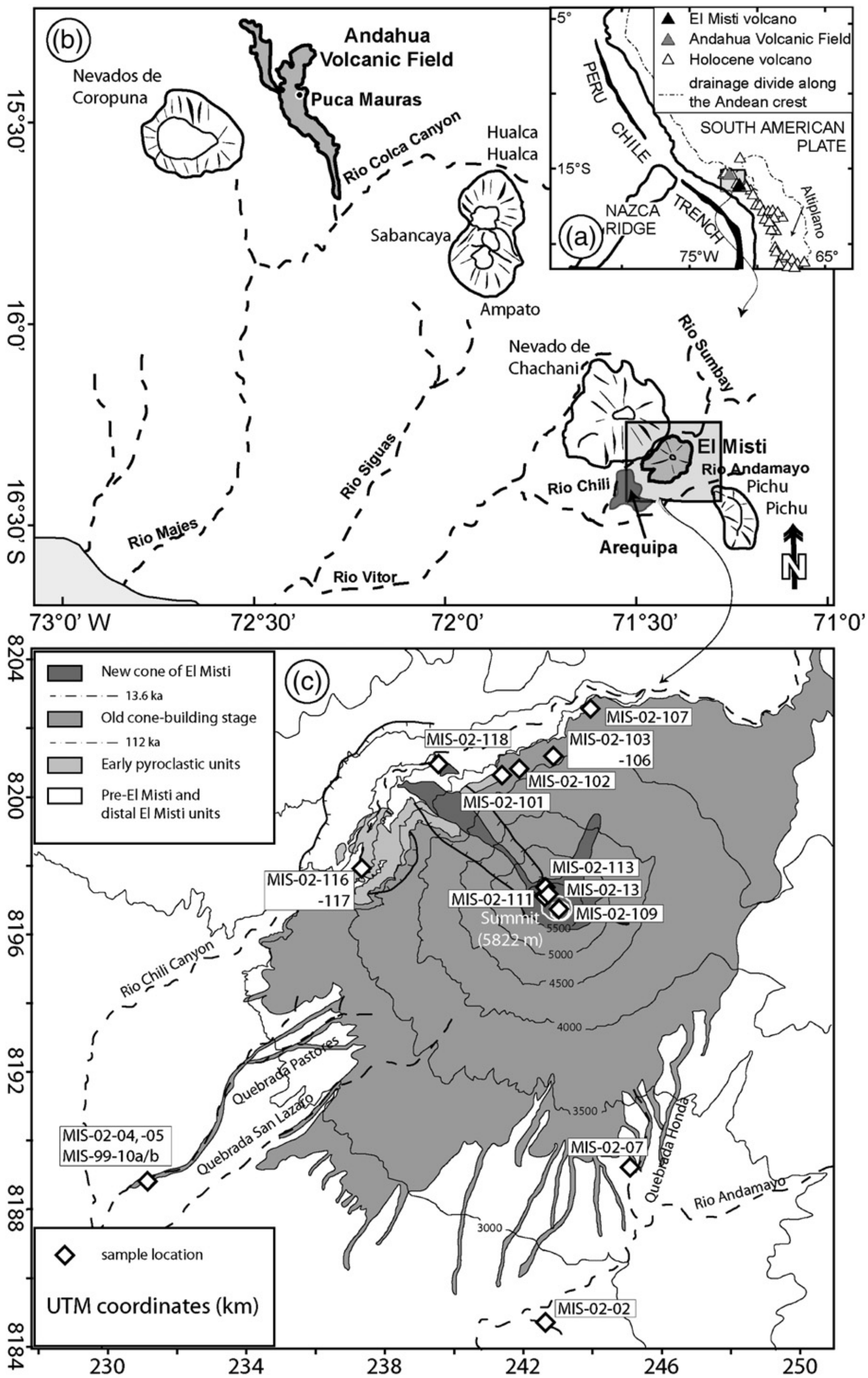

Fig. 1. a) Locations of the Andahua Volcanic Field (AVF) and El Misti stratovolcano in the South Peruvian part of the Central Andean Volcanic Zone. b) The Puca Mauras monogenetic cinder cone (AND01, AND08 and AND10) is the largest center within the "Andanhua Valley of Volcanoes". c) Sample location map of El Misti (geologic map after Thouret et al., 2001, and field mapping of the authors).

Cinder cones and lava flows are produced by strombolian eruptions, which resulted in steep-sided cones and abundant blocky lava flows (de Silva and Francis, 1991; Delacour et al., 2007).

2.1. Stratigraphy of El Misti volcano and sampling

Locally derived ignimbrites and other volcaniclastic deposits form the base on which the El Misti edifice is built (Paquereau-Lebti et al., 2006). Its cone is subdivided by a major unconformity at ~5500 m marking the change from the main old-cone-building stage and the new cone. The age of the unconformity has been reported by Thouret et al. (2001) to be 13.6 ka.

Following Thouret et al. (2001), the base of El Misti is formed by non-welded scoria flows and volcaniclastic sediments, followed by a series of 50 m thick, flow-banded lava flows dated at 833 ka (K–Ar whole rock). However, we argue that these older deposits and the lower lava flow sequence may not be related to El Misti for the following reasons: (1) These lavas are petrographically clearly distinct (aphyric) from typical El Misti lavas; (2) if these flows belonged to El Misti then there would be an unlikely large break in history between this 833 ka old lava and next the overlying lava flows dated at 112 ka (Thouret et al., 2001) only separated by two units of proximal dacitic pyroclastic deposits. These most likely originated from El Misti volcano, indicating that El Misti probably started off as a dome complex with a pyroclastic apron. We then suggest that the present El Misti stratovolcano and the main cone-building eruptions are only slightly older than 112 ka, i.e. the lowest lava flow dated by Thouret et al. (2001) to overly these early El Misti deposits.

During the new cone-building stage from 13.6 ka onwards, above the unconformity at 5500 m, two nested inner craters developed at the present summit (5822 m). Their andesitic lava and tephra deposits cover the summit and upper flanks of El Misti. The most recent effusive activity is represented by a thick andesitic dome-like plug and abundant fumaroles inside the inner crater. In historic time only fumarolic and phreatic activity has been reported (Thouret et al., 2001).

66 samples representing the entire eruptive history of El Misti volcano have been taken from the Quebradas Honda and Pastores, the Rio Chili Canyon and the flanks and the summit of El Misti volcano. A set of 20 samples was processed for whole rock and analysed for major and trace elements (Fig. 1; Table 1). Detailed microprobe work was performed on phenocrysts of these 20 samples (for entire data set see supplementary material).

2.2. Andahua Volcanic Field

Delacour et al. (2007) describe the Andahua Volcanic Field in detail. The AVF contains about 40 cones, most of which are located on the valley floor. The total volume of the volcanics is estimated to be around 15±5 km^3 with a maximum accumulated lava thickness of 130 m. A total of 16 samples have been analyzed for whole rock major and trace elements. Andahua samples are crystal-poor containing <10% total phenocrysts. Most samples have similar relative abundances of plagioclase > clinopyroxene > olivine > orthopyroxene > Fe–Ti oxides. Hornblende is restricted to andesitic compositions (Delacour et al., 2007). Plagioclase phenocrysts are characterized by two distinct growth zones: a sodic core is overgrown by a calcium-rich rim. Three samples from Andahua have been investigated in this study: AND-99-01, AND-99-08, AND-99-10. All three samples represent different flows of the Late Holocene Puca Mauras volcano, the largest center in this field (Delacour et al., 2007).

3. Analytical techniques

Major- and minor-element (Si, Ti, Al, Fe, Mn, Mg, Ca, Na, K, P) abundances were measured by X-ray fluorescence spectroscopy (XRF) on fused glass discs on a Philips PW 1480 XRF spectrometer at the Abteilung Geochemie, Geoscience Center Goettingen. Based on multiple measurement of internal and international reference material (BB, GD) the analytical error for both major and minor-elements is ±0.4–1.8%. After petrographic examination detailed electron microprobe work was performed using a JEOL 8900 RL following procedures described by Ginibre et al. (2002a) and Triebold et al. (2006). Plagioclase zonation is documented in BSE images where BSE intensity increases with An content. An profiles were extracted based on grey-scale calibrated BSE images. Major (Si, Al, Ca, Na, K), minor (Ba, Sr, Fe) and trace (Ti, Mg) quantitative point measurements of particular zones in plagioclase from El Misti volcano were performed at 15 kV acceleration voltage, 40 nA beam current and a beam size of 10 µm. Peak counting times for major elements other than Ca (30 s) were 15 s and for minor and trace elements were either 150 s (Ba, Ti, Fe) or 300 s (Mg, Sr) (trace mode). To provide complete plagioclase microprobe analyses all elements are presented in the supplementary data set. However, this paper specifically deals with the Fe–Mg and An contents in these plagioclases. Tests with variable beam currents to assess Na loss were performed on homogenous plagioclase. Despite the high current no significant Na loss was detected when analyzing the alkali elements first. Measurements were performed directly inboard and outboard of major resorption interfaces. Contrasts between cores and rims were large for Andahua samples, therefore lower precision measurements were sufficient. For these samples measurements were performed at 15 nA beam current

Table 1
Location, ages, rock types, whole rock, and glass compositions for samples from El Misti volcano

	Whole rocks										
Sample	MIS-02-109	MIS-02-13	MIS-02-118	MIS-02-111	MIS-02-113	MIS-02-04	MIS-02-02	MIS-99-10A	MIS-99-10B	MIS-02-05	MIS-02-07
Age (ka) [b]	Historic	<1.5	1.5–13.6	1.5–13.7	c. 13.7	~34	14–25	34	34	~48	~49
Rock type	Andesite plug	Dense andesite	Andesite flow	Andesite flow	Andesite flow	Grey pumice from scoria flow	Rhyolitic pumice	Mixed pumice from scoria flow	Mixed pumice from scoria flow	Andesite from dome collapse breccia	Andesite flow
Locality	Inside active crater	Bomb from explosion breccia near summit	Young flow into Rio Chili	Near crater above unconformity	Near crater above unconformity	Queb. Pastores	Chiguata Surge	Queb. Pastores	Queb. Pastores	Base of section Queb. Pastores	Queb. Aguada Salada
Major elements [wt.%]											
SiO_2	58.10	58.00	57.10	59.20	58.30	58.40	68.67	58.00	59.50	61.20	60.40
TiO_2	0.89	1.00	0.94	0.79	0.86	0.72	0.19	0.89	0.73	0.62	0.75
Al_2O_3	16.70	16.90	17.20	17.40	17.10	16.80	14.30	17.20	17.50	17.00	17.10
FeO	6.69	6.15	6.24	5.61	5.75	5.22	1.31	5.90	5.49	4.65	5.29
MnO	0.12	0.10	0.10	0.09	0.09	0.09	0.09	0.10	0.10	0.09	0.10
MgO	3.15	3.83	3.54	2.94	3.29	2.88	0.45	3.32	2.94	2.29	2.63
CaO	5.88	6.03	6.34	5.66	5.39	5.34	1.46	5.97	5.75	4.79	5.36
Na_2O	4.28	4.09	4.13	4.23	4.01	3.78	4.38	4.30	4.18	4.32	4.48
K_2O	1.81	2.29	2.11	2.22	2.42	2.13	3.64	2.08	2.13	2.53	2.24
P_2O_5	0.29	0.33	0.31	0.27	0.30	0.25	0.14	0.30	0.25	0.25	0.28
Trace elements [ppm]											
Nb	5	9	4	5	5	6	8	4	6	8	4
Zr	168	188	165	158	184	158	129	162	146	179	171
Y	13	16	10	13	15	10	10	14	13	19	14
Sr	834	932	890	860	894	772	348	862	786	813	822
Rb	28	45	40	44	53	42	74	35	38	12	41
Ga	22	22	24	22	23	24	16	22	20	22	22
Zn	101	88	85	84	90	84	53	80	74	76	84
Cu	36	78	96	96	156	81		77	68	53	70
Ni	15	45	31	22	33	23	2	31	23	17	18
Co	21	25	22	24	23	18		20	18	12	22
Cr	22	65	27	22	57	45	6	57	25	20	15
V	152	164	164	137	151	127	8	147	125	100	126
Ba	881	1059	931	978	1114	978	1109	983	935	1128	1013
Sc	16	20	20	15	13	17	1	13	16	12	8

[a] Glass compositions from multiple microprobe analyses, N=number of analyses.
[b] Ages according to Thouret et al. (2001).

and a beam size of 5 μm at the same acceleration voltage. Peak counting times ranged between 15 and 30 s (major-element mode). 2σ errors for the 393 trace mode measurements average 1.1+/−0.10% and 4.2+/−1.1% for Ca and Fe, respectively. For major-element mode analyses the 2σ errors average 1.8+/−0.42% and 13.5+/−5.5%, respectively.

4. Results

4.1. Geochemistry

El Misti volcanics fall near the boundary of typical Quaternary, high-K calc-alkaline volcanics and the medium-K field (Fig. 2). Whole rocks are mostly andesite to

									Glass[a]		
MIS-02-106 70–112	MIS-02-105 70–112	MIS-02-104 70–112	MIS-02-103 70–112	MIS-02-102 70–112	MIS-02-101 70–112	MIS-02-107 ~112	MIS-02-116 >112	MIS-02-117 >112	MIS-02-109 Historic	MIS-02-104 70–112	MIS-02-117 >112
Andesite flow	Grey mixed pumice	Black andesite scoria	Andesite flow	Andesite flow	Andesite flow	Andesite flow	Andesite block from breccia	Andesite scoria flow	Andesite plug	Black andesite scoria	Andesite scoria flow
Upper Queb. Rio Chile, base of cone	Upper Queb. Rio Chile, base of cone	Upper Queb. Rio Chile, base of cone	Upper Queb. Rio Chile, base of cone	Upper Queb. Rio Chile, base of cone	Upper Queb. Rio Chile, base of cone	Upper Queb. Rio Chile, base of cone	Middle Queb. Rio Chili	Queb. Rio Chili	Andesite plug inside active crater	Upper Queb. Rio Chile, base of cone	Queb. Rio Chili
									$N=5$	$N=4$	$N=4$
62.30	58.30	58.10	60.00	60.20	61.50	59.20	58.30	59.10	69.96	62.27	68.08
0.55	0.80	0.90	0.75	0.76	0.68	0.78	0.87	0.82	0.77	0.75	0.63
17.40	16.90	17.10	16.90	17.20	16.90	17.40	17.00	16.70	12.94	16.54	14.90
4.41	5.45	5.80	5.31	5.37	5.05	5.54	6.08	5.45	3.00	4.21	2.61
0.10	0.09	0.09	0.09	0.10	0.10	0.09	0.10	0.09	0.07	0.08	0.05
1.69	3.07	3.29	2.80	2.78	2.66	2.66	3.25	3.05	0.39	1.67	0.74
4.81	5.70	6.03	5.46	5.42	5.10	5.65	5.97	5.48	0.83	3.89	2.05
4.52	4.01	4.31	4.07	4.29	4.12	4.04	4.04	4.19	4.53	4.81	4.55
2.47	2.20	2.20	2.46	2.25	2.43	2.26	2.13	2.27	4.76	3.02	4.25
0.28	0.27	0.30	0.27	0.27	0.24	0.31	0.27	0.27			
7	8	6	8	6	8	8	6	8			
188	163	181	175	164	161	163	162	165			
11	13	12	10	14	12	10	13	15			
833	826	910	806	797	752	868	785	787			
53	47	42	46	43	48	43	40	42			
20	21	23	22	23	22	22	24	23			
80	85	87	84	77	72	104	88	77			
28	68	78	49	81	62	48	81	58			
4	24	29	24	18	17	15	25	25			
12	27	21	17	17	19	21	25	27			
3	26	40	39	22	26	23	34	38	0.55	0.66	0.95
80	147	147	122	125	118	123	152	134			
1074	968	1028	1080	982	1021	990	916	980			
10	12	16	14	15	13	17	15	17			

silicic andesite in composition (Table 1). AVF rocks are all high-K, calc-alkaline. They are distinct in major-element composition from El Misti by their higher K_2O and FeO*/MgO ratios at a given silica content.

Major-element compositions for plagioclases are presented in the supplementary data. Most El Misti plagioclases have intermediate plagioclase compositions ranging from An40 to An80, some are more restricted (Fig. 3). The rhyolitic pumice of the Chiguata Surge (MIS-02-02) has feldspars with lowest An contents of An20 to An30.

The plagioclases from Andahua lavas range from An30 to An60. The cores are lower in An than the rims (Fig. 3j) producing a bimodal compositions of cores and rims.

4.2. Plagioclase growth pattern

A total of 398 different plagioclases were imaged with BSE technique from which only a small representative selection of the major types of growth patterns is presented here (Fig. 3) (A comprehensive image collection is available as Image CD upon request from the first author). There are large variations in growth textures within and between samples, but feldspars selected here cover the important types and are representative for the large sample set of the volcano. Multiple plagioclase types have been identified in most samples from El Misti (Table 2). In contrast, AVF lavas are characterized by one single population only.

Fig. 3 shows BSE images of thirteen typical plagioclase phenocrysts from three samples. Many samples are characterized by plagioclase with complex resorption and growth features, e.g. MIS-02-102 (Fig. 3a–d), MIS-02-05 (Fig. 3e–i). By contrast the sample from the Recent El Misti plug (MIS-02-109; Fig. 3k–n) and samples from Andahua Volcanic Field (Fig. 3j) have surprisingly simple and similar growth patterns. (Table 1).

The most common core features are (1) sieved-textured, (2) high An, sometimes partly resorbed, (3) low An and (4) normally zoned. Cores can have several of those features combined, with the exception of mutually exclusive features, like low vs. high An. Plagioclase populations with high An cores of (1) and (2) occur in all studied rocks from the entire stratigraphic sequence. The cores typically comprise up to 50% of the distance from core to rim. Rims and mantles are much more variable and can be characterized by their distinct resorption and growth features. Resorption features include (5) rough and irregular interfaces, (6) sharp and straight interfaces, (7) resorption–regrowth zones similar to sieve-textures, and (8) narrow growth bands with an An saw-tooth pattern. These saw-tooth patterns are characterized by multiple normally zoned growth bands separated by subtle resorption interfaces, where the An contents suddenly jump back to high An. Further growth features are divided into (9) reverse trend, (10) An spikes, (11) high-frequency oscillatory variations, (12) low-frequency variations, (13) low amplitude variations, (14) step-wise zonation, (15) homogeneous An content and (16) low An contrasts. The crystal shape also indicates whether the final stage was dominated by growth (17: euhedral) or by resorption (18: anhedral). Major resorption events are characterized by a large sudden increase in An content. A table with crystal size information as well as visually based resorption event interpretations for the investigated phenocrysts is available in the supplementary data set.

Amphibole is present in most samples. Sometimes it is chemically zoned, though it is much more homogeneous than plagioclase based on BSE images and unpublished major-element composition data. Several tens of micron thick reaction rims associated with the breakdown of amphibole to plagioclase, magnetite, pyroxene and melt is predominant in the samples. However, a few samples lack such reaction rims completely. Of particular interest in this respect is a scoria from Quebrada Pastores (MIS-99-10a and MIS-99-10b). These two samples show macroscopic signs of mixing, where sample MIS-99-10a is the mafic and MIS-99-10b the silicic end-member. Indicative for a mafic recharge are the pristine amphibole crystals in MIS-99-10a, while the amphiboles from the silicic mixing end-member do have breakdown rims. Therefore, the silicic was resident for some time under shallow conditions (Fig. 4).

4.3. An–Fe systematics of El Misti plagioclase phenocrysts

Iron–anorthite systematics lend themselves to separating chemical versus thermal effects of magma mixing (Ginibre et al., 2002a). Fe is not a major element in feldspars; its concentration depends only on melt composition and degree of oxidation. We put particular focus on the Fe-trace element composition in those growth zones that lie outboard of a resorption event towards the rim because we expect valuable information on the causes of resorption from these data.

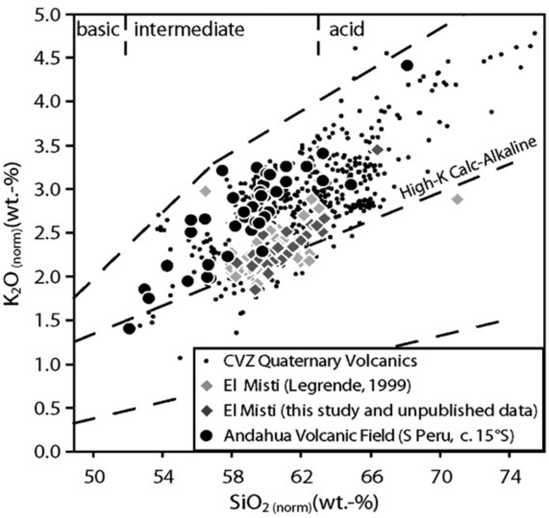

Fig. 2. Alkali-silica diagram normalized to 100% for samples from El Misti, Andahua Volcanic Field and volcanic centres from the Central Andean Volcanic Zone (G. Wörner, unpublished data set). Most samples are high-K calc-alkaline. Andahua samples (from Delacour et al. (2007)) have high K_2O for a given SiO_2-content.

Representative An profiles for El Misti volcano and corresponding Fe concentrations for spot measurements for thirteen plagioclases from MIS-02-102 and MIS-02-05, MIS-02-109 are given in Fig. 3.

The simple-textured plagioclases of the plug (MIS-02-109) are characterized by a single main resorption zone with a jump from An40 to An60. Minor resorptions in the core are associated with only a slight increase in An content. The major resorption event is correlated with a 3-fold increase in Fe (Fig. 3k–n), while the minor ones do not show significant Fe variations (Fig. 3n).

A second set of An profiles belongs to plagioclase phenocrysts of MIS-02-102 (Fig. 3a–d), a lava from close to the base of the El Misti sequence. These phenocrysts share a few features observed in MIS-02-109. In particular, some phenocrysts have one major resorption (Plg2 and Plg16). A second type has slightly more complex crystals (Plg4 and Plg14), comprised of multiple resorption events. Fe content is increasing across the major resorption interfaces by a factor of 2 for crystals like Plg2 and Plg16. More complex crystals (Plg4 and Plg14) also show an increase in Fe concentration towards the rim, though more gradual and with a smaller total variation.

Phenocrysts of MIS-02-05 (Fig. 3e–i) are also complexly zoned. Up to eight resorption events have been identified with maximum An contrasts of 20 mol%. However, in contrast to El Misti plug (MIS-02-109) and MIS-02-102, no Fe variations are associated with the frequent resorption interfaces. Instead, Fe concentrations scatter around 0.4 wt.%.

5. Discussion

5.1. Magmatic processes recorded in An zonation pattern

Crystallisation at El Misti occurs around 900 to 950 °C and 2 to 3 kbar with oxygen fugacities varying from −12.3 to −10.8 for log fO_2 (Legrende, 1999). Maximum water solubility for andesitic to dacitic magmas ranges from 5.1 wt.% to 6.0 wt.% using a standard Burnham model (Burnham, 1994; Holloway and Blank, 1994). For limited late-stage degassing water-undersaturation of El Misti magmas is assumed.

Plagioclase crystallisation can either be caused by decompression/degassing or by cooling (Nelson and Montana, 1992; Hammer and Rutherford, 2002). Therefore, An variations in plagioclase are potentially

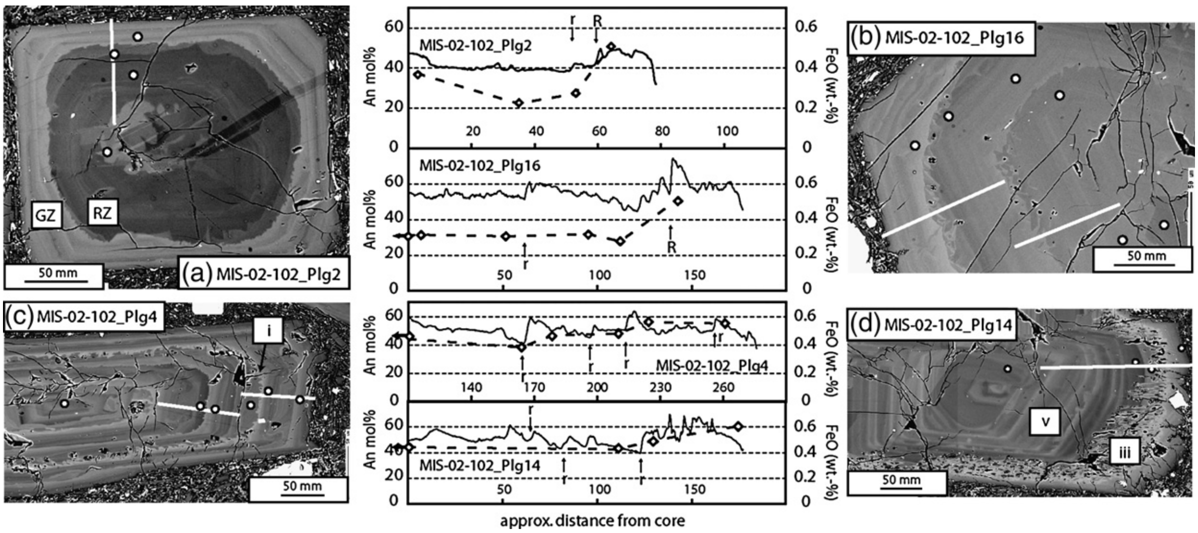

Fig. 3. BSE images, An profiles and Fe concentration of plagioclase phenocrysts from (a–d) MIS-02-102 (early El Misti), (e–i) MIS-02-05 (<34 ka) and (k–n) MIS-02-109 (plug). The plagioclase population of the plug is very similar to phenocryst populations from the monogentic cones in the Andahua Volcanic Field (Fig. 3j; see also Fig. 7, Table 2). White points and lines represent spot measurements and An profile sampling, respectively. Some of the main growth features are displayed in these phenocrysts: i, rough interface; ii, sharp interface; iii, resorption–regrowth zone; iv, saw-tooth pattern; v, low-frequency variations. The term resorption zone (RZ) corresponds to a zone directly inbound of a resorption interface. Growth zone (GZ) consequentially refers to a growth zone just outbound of a resorption interface. Note the Fe concentration variation across resorption features. MIS-02-109 and MIS-02-102 is dominated by An–Fe correlations, MIS-02-05 shows small, almost constant Fe concentrations with changing An content. (R) (An and Fe variation) and (*r*) (only An variation) in the An profiles mark resorption events identified in the BSE images.

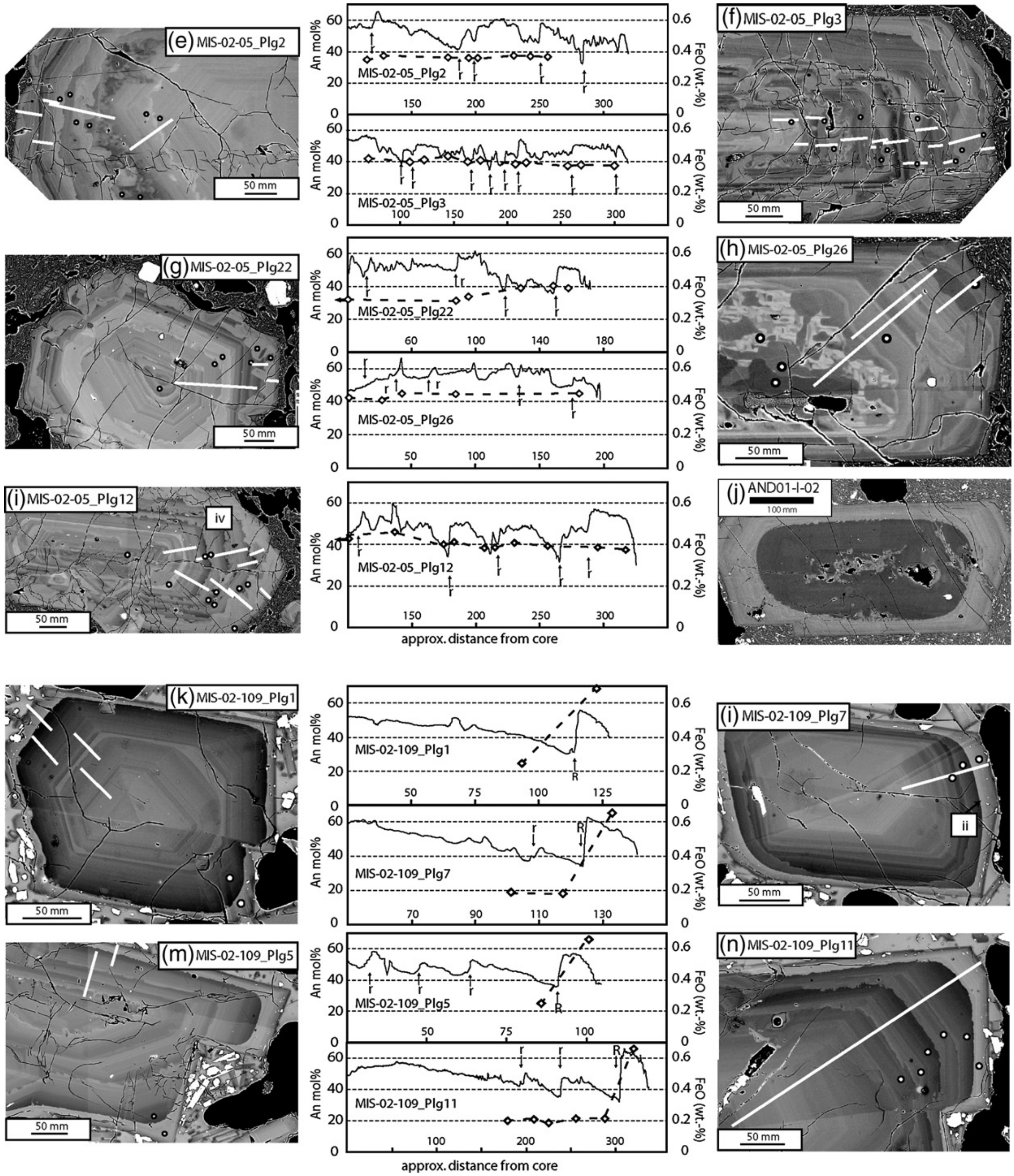

Fig. 3 (*continued*).

controlled by temperature, pH_2O and magma composition. With higher pH_2O and/or higher temperature plagioclase An contents will be higher. Lithospheric pressure, however, has little effect on plagioclase at a given liquid composition (Housh and Luhr, 1991; Brown and Parsons, 1994).

Three main mechanisms can be responsible for compositional variations in plagioclase assuming that the

Table 2
Open vs. closed-system behaviour. Samples are in stratigraphic order, for compositional data and ages see Table 1

Sample	Rock type	Deposit	Average (ΔFe/ΔAn) resorption [a]	Open vs. closed behaviour [b]	Plagioclase populations
MIS-02-109	Andesite plug	Inside active crater	0.039	Open	1
MIS-02-13	Dense andesite	Bomb from explosion breccia near summit	0.006	Mainly closed (one phenocrysts shows late open-system)	2
MIS-02-118	Andesite flow	Young flow down into Queb. Rio Chili	0.008	Mainly closed (one phenocrysts shows late open-system)	2
MIS-02-111	Andesite flow	Near crater above unconformity	0.035	Late-stage open	2
MIS-02-113	Andesite flow	Near crater above unconformity	0.018	Late-stage open	2
MIS-02-04	Grey pumice from scoria flow	Queb. Pastores	0.001	Closed	2
MIS-02-02	Dacite pumice	Queb. Pastores			1
MIS-99-10a	Mixed pumice from scoria flow	Queb. Pastores	0.013	Open	5
MIS-99-10b	Mixed pumice from scoria flow	Queb. Pastores	0.009	Open	3
MIS-02-05	Andesite from dome collapse breccia	Base of section Queb. Pastores	0.001	Closed	3
MIS-02-07	Andesite flow	Queb. Aguada Salada	0.002	Closed	3
MIS-02-106	Andesite flow	Upper Queb. Rio Chile, base of cone	0.002	Closed	3
MIS-02-105	Grey mixed pumice	Upper Queb. Rio Chile, base of cone		Not enough measurements	1
MIS-02-104	Black andesite scoria	Upper Queb. Rio Chile, base of cone	0.003	Closed	2
MIS-02-103	Andesite flow	Upper Queb. Rio Chile, base of cone	0.016	Minor open (two phenocrysts in mantle)	3
MIS-02-102	Andesite flow	Upper Queb. Rio Chile, base of cone	0.016	Open	3
MIS-02-101	Andesite flow	Upper Queb. Rio Chile, base of cone	0.009	Open	4
MIS-02-107	Andesite flow	Upper Queb. Rio Chile, base of cone	−0.002	Closed	2
MIS-02-116	Andesite block from breccia	Middle Queb. Rio Chili	0.061	Mainly open	2
MIS-02-117	Andesite scoria flow	Queb. Rio Chili	0.002	Closed	3
AND01	Andesite flow	Puca Mauras Cone	0.035	Open	1
AND08	Andesite flow	Puca Mauras Cone	0.015	Open	1
AND10	Andesite flow	Puca Mauras Cone	0.015	Open	1

[a] Average is calculated from single An–Fe slope across major resorption events in Fig. 7.
[b] Inferred from average An–Fe slope.

magma system beneath El Misti volcano consists of one major interconnected reservoir:

(1a) Decompression during magma ascent may occur in distinct steps resulting in variable An contents during crystallisation. Decompression–crystallisation can cause heating of the magma due to release of latent heat (Blundy et al., 2006) and thus also lead to increasing An contents during plagioclase crystallisation. Stagnation, subsequent cooling and– in rare cases– degassing at the water-saturation point may lead to lower An content. Since ascent and degassing also results in the breakdown of amphibole (Rutherford and Hill, 1993), we will also shortly consider such evidence for amphibole destabilisation below to better constrain the causes of plagioclase resorption events.

(1b) Underplating of a recharge magma that provides only heat to the host magma and causes thermal convection (plumes) within the overlying, more evolved magma (Couch et al., 2001). Concurrently, cold plumes may generate in crystal-laden areas within the magma and descend into lenses with higher melt content (Marsh, 1989; Singer et al., 1995; Triebold et al., 2006). These crystal-laden plumes may transport crystals from the cooler boundary layer into the main melt volume (Marsh, 1988; Jaupart and Tait, 1995). Couch et al. (2001) used the term “self-mixing” for this process. Since thermal effects dominate convection leading to mixing of magmas with different temperatures but only low compositional contrast, we prefer the term “thermal mixing”. Depending on the time scales of mixing and crystallisation An contents will vary during such “thermal mixing” in the phenocrysts and record for short mixing time scales only the initial and final thermal conditions. For prolonged mixing processes transient variations may also be recorded. Amphibole is less affected by a temperature increase from underplating magma unless temperatures in the host magma exceed its stability conditions. Nevertheless, the preservation of amphibole during a replenishment event cannot rule out the mechanism of hotter more mafic intrusions as viable for the evolution of El Misti magmas since observed breakdown rims in amphibole can be caused much later during ascent. It has been shown that reaction rims in amphibole develop within days to weeks (Rutherford and Hill, 1993).

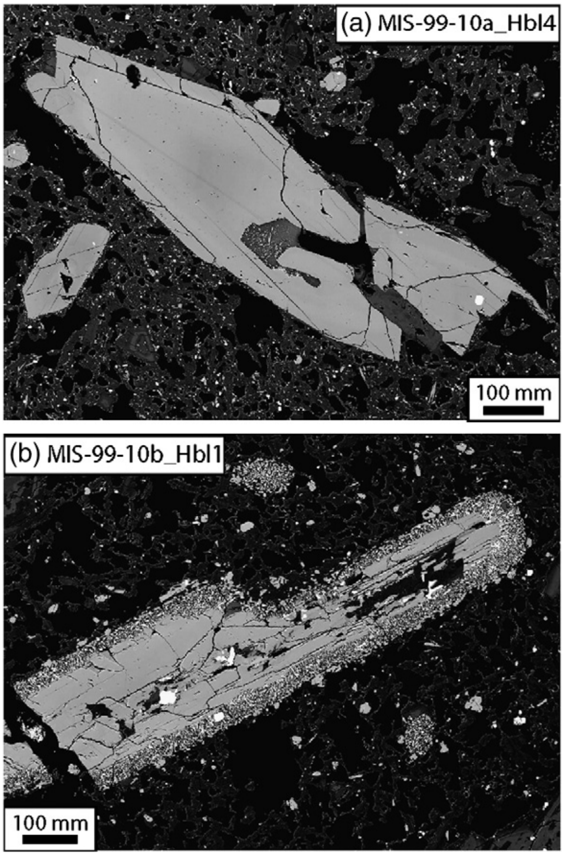

Fig. 4. Amphibole in the (a) mafic MIS-99-10a and the (b) silicic MIS-99-10b. The amphiboles in the silicic samples show prominent reaction rims.

(2) Mixing with chemically different magma is a modification of mechanism (1b). While underplating only causes heat transfer to the host magma and mass transfer is restricted to volatiles, mixing with recharge magma may also include mass transfer of liquid and solid phases. Therefore, this mechanism will generate An variations due to temperature variations as well as to composition. Possible mechanisms have been proposed by Bergantz and Breidenthal (2001) and Snyder and Tait (1996) envisioning vesiculation of the mafic magma and convective entrainment due to viscous drag. This mechanism is here called “compositional mixing”.

In summary, An variations during plagioclase crystallisation within the magma are expected for both, closed-system (heat transfer and decompression) and open-system processes (recharge), and therefore An variations alone cannot distinguish between closed and open-system behaviour.

5.2. Do fO_2 variations in El Misti magmas affect Fe in plagioclase phenocrysts?

Closed- or open-system effects on magma evolution can be recorded by trace element composition in plagioclase. For example, constant compositions in the host melt will be reflected by constant trace element contents in the plagioclase, even though the plagioclase may have variable An due to changes in T and H_2O-content. If, by contrast, trace elements change with variable An, then zonations will reflect chemically open-system behaviour.

Trace elements incorporated into plagioclase can be divided into two groups: (1) elements that take part in substitution reactions (e.g. Sr for Ca in plagioclase), and (2) elements that are mostly incorporated since they are major components of the liquid (e.g. Fe or Mg in plagioclase) but do not easily fit onto a lattice site based on the elastic-strain model of Blundy and Wood (1994).

The concentrations of the second group of trace elements in plagioclase, e.g. Fe and Mg, depend mostly on the concentration of the element in the host melt (Ginibre et al., 2002a,b). In addition, Bindeman et al. (1998) and Wilke and Behrens (1999) have shown that Fe partitioning into plagioclase is strongly dependent on the oxygen fugacity fO_2, temperature, An- and H_2O-content. Based on their data Fe partitioning for plagioclase should decrease for decreasing fO_2, and increase with temperature and An content. Thus, Fe and An should be inversely correlated for constant fO_2.

Integrating fO_2-independent Mg data from El Misti with Fe data provides the important constraints. Sugawara (2000, 2001) present evidence for only minor K_D variation at constant oxygen fugacity of Mg and Fe in plagioclase over the entire range of An content ($K_{Mg,Fe}^{Plg}$). Thus, the Mg–Fe pair is suitable to assess variations in fO_2. An independent test of the fO_2 variations can also be done using experimental data of Bindeman et al. (1998) and Wilke and Behrens (1999). Key parameters that are used to assess the effect of fO_2 variations on Fe partitioning in plagioclase are given in Table 3.

Our data show a similar behaviour for Mg and Fe in plagioclase of El Misti (Fig. 7). The majority of crystals analysed show flat to slightly positive correlations between An and Fe. An and Mg are weakly negatively correlated. The effect of changing fO_2 on Fe contents will now be assessed based on published experimental studies. For this, we assume a constant Fe/Mg ratio in the liquid and a constant K_D for Mg and Fe in plagioclase for a given fO_2. Using the linear relationship between fO_2 and $K_{Mg,Fe}^{Plg}$ (Sugawara, 2001; Fig. 3) at ΔQFM-5 to 5 we calculate the limits of possible changes in fO_2 from the observed An–Fe variations (Fig. 7) to be only 0.9 to 2.0 log units. An independent estimate is based on experimental D_{Fe} data of Bindeman et al. (1998) which we modified to the form:

$$1n\ D_{Fe} = 7.59 + 8.2\ 10^{-5}\text{An[mol\%]} + 6.2 \cdot 10^{-3} T[K]. \quad (1)$$

Given the observed An values and temperatures consistent with the El Misti system (Table 2) results in a discrepancy of 0.14 and 0.28 $\Delta \log D_{Fe}$ between observed trends in Fig. 7 and $\log D_{Fe}$ calculated from the Bindeman et al. (1998) data. This corresponds to a maximum fO_2 variation of 0.9 to 1.7 log units fO_2, respectively (Wilke and Behrens, 1999; Fig. 5b). Thus our result using the combined Bindeman et al. (1998) and Wilke and Behrens (1999) studies is in good agreement with the independent estimate based on Sugawara (2000, 2001), and both are consistent with 1.5 log unit fO_2 variations deduced from whole rock samples by Legrende (1999).

Table 3

a: Model parameters in plagioclase to assess fO_2 variations on Fe content based on Sugawara (2001)

	Prior resorption	After resorption
An [mol%]	40	75
MgO [ppm]	520	400
Mg [µmol/g]	13	10
Horizontal case [a]		
FeO [wt.%]	0.425	0.433
Fe [µmol/g]	59	60
$(Fe/Mg)_{Plg}$	4.6	6.1
$(Fe/Mg)_{An75}/(Fe/An)_{An40}$		1.3 [b]
$\Delta \log(fO_2)$		0.9 [b]
Slightly positive case [a]		
FeO [wt.%]	0.425	0.600
Fe [µmol/g]	59	83
$(Fe/Mg)_{Plg}$	4.6	8.4
$(Fe/Mg)_{An75}/(Fe/An)_{An40}$		1.8 [b]
$\Delta \log(fO_2)$		2.0 [b]

b. Model parameters in plagioclase to assess oxygen fugacity variations on Fe content associated with changes in temperature based on Bindeman et al. (1998) and Wilke and Behrens (1999)

	Prior resorption	After resorption
An [mol%]	40	75
T	900	950
$\log D_{Fe}$ [c]	0.149	0.016
Horizontal case [a]		
FeO [wt.%]	0.425	0.433
Fe $[\mu mol/g]_{obs}$ [d]	59	60
Fe $[\mu mol/g]_{liq}$ [e]	42	
Fe $[\mu mol/g]_{const\,fO2}$ [f]		44
$\Delta \log(fO_2)$		0.9 [g]
Slightly positive case [a]		
FeO [wt.%]	0.425	0.600
Fe $[\mu mol/g]_{obs}$ [d]	59	83
Fe $[\mu mol/g]_{liq}$ [e]	42	
Fe $[\mu mol/g]_{const\,fO2}$ [f]		44
$\Delta \log(fO_2)$		1.7 [g]

[a] Trends are taken from Fig. 7d.
[b] Relationship between $(Fe/Mg)_{An75}/(Fe/An)_{An40}$ and $\Delta \log(fO_2)$ taken from Fig. 3 of Sugawara (2001) using a linear approximation for the data from ΔQFM −5 to +5.
[c] Partition coefficient taken from Eq. (1).
[d] Based on trend from Fig. 7d.
[e] Using partition coeff. from Eq. (1) and observed Fe content in plag at An40.
[f] Calculating the equilibrium Fe concentration assuming constant oxygen fugacity and Fe content in the liquid.
[g] Relationship between D_{Fe} and $\Delta \log(fO_2)$ taken from Fig. 5b of Wilke and Behrens (1999).

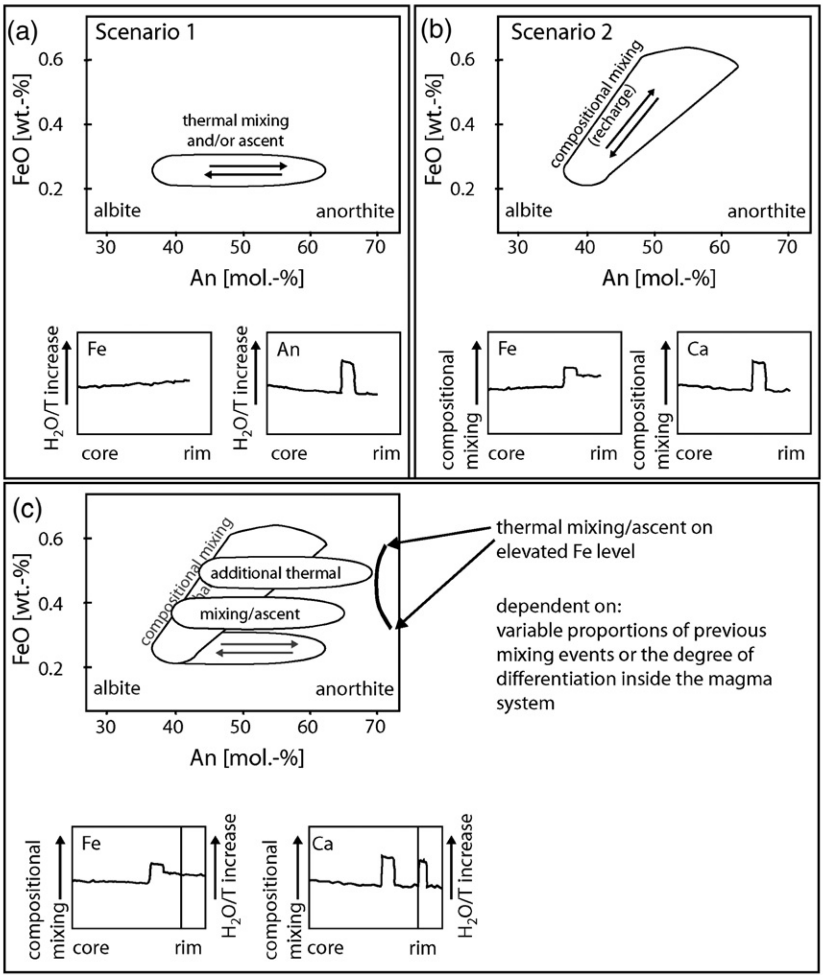

Fig. 5. An–Fe patterns for closed- and open-system scenarios. a) In the thermal mixing and ascent scenario the Fe content is not affected, while An varies due to temperature or pH_2O variations. The small figures at the bottom correspond schematically to the Fe and An concentration profiles for simplified exemplary plagioclase that experiences one resorption event. b) An–Fe patterns for the compositional mixing scenario. Fe and An concentrations are both affected in the compositional mixing model. c) Combined An–Fe pattern for thermal mixing and compositional mixing. Thermal mixing or ascent can occur on different Fe levels. This is dependant on variable proportions of previous mixing events or the degree of differentiation inside the magmatic system.

Positively correlated trends for An and Fe steeper than those just discussed cannot be simply explained by changes in temperature, fO_2 or pH_2O. Thus other processes such as compositional variations during differentiation (or recharge and mixing) must be considered.

After Behrens et al. (1990) and Costa et al. (2003) diffusion rates of Fe^{3+} are about 3 orders of magnitude slower than that of Mg implying that Mg should reach equilibrium well before Fe. At full equilibrium Mg should show strong negative correlations with An (Bindeman et al., 1998), which is not observed for most plagioclases at El Misti. Thus, Mg has not yet equilibrated suggesting that Fe could not have been significantly affected by diffusion. An important conclusion from this discussion is that both, Mg and Fe can be used as a proxy for the degree of differentiation in the melt (Ginibre et al., 2002b; Costa et al., 2003).

5.3. Models to explain An–Fe variations

This section focuses on the combined An–Fe variations and discusses models that are consistent with trace element variations observed in El Misti and AVF samples. An–Mg variations can be interpreted in a similar way. The three mechanisms introduced in Section 5.1 are now discussed in more detail with respect to the trace element variations. However, one question has to be answered first: Why is simple forward fractional crystallisation not considered as a main mechanism for explaining the Fe–An compositions in El Misti plagioclase? Changes in Fe contents of the melt could also be caused by crystallisation of the main phases in these magmas — plagioclase, pyroxene and amphibole, Fe–Ti-oxides. To increase the iron content in the melt by a factor of 1.5, more than 20% of additional plagioclase crystallisation is necessary. This is based on mass balance calculations from whole rock-data and microprobe analyses of the present phases. Such large percentages of crystallisation, however, force the magma to dacitic or rhyodacitc compositions. These compositions are rare at El Misti. Pyroxene, amphibole and Fe–Ti oxide crystallisation are not capable of elevating the Fe concentration in the melt, since they have a partitioning for Fe larger than 1. Therefore, simple fractional crystallisation is not further considered for the Fe variations in plagioclase patterns observed at El Misti and Andahua.

Thus we are left with two end-member scenarios (closed- vs. open-system) to explain An–Fe zonation patterns (Fig. 5):

(1a) Plagioclase will crystallize a more anorthitic composition after an increase in pH_2O due to decompression-induced reheating (Blundy et al., 2006). Subsequent cooling, degassing and adjustment to a new pH_2O may cause the An content to continuously decrease until another decompression event. Fe compositions remain at similar concentration over this growth interval (Fig. 5a) only modified by small adjustments of fO_2 due to changes in temperature and water content.

(1b) The same chemical effect is associated with "thermal mixing" (Fig. 5a). If the plagioclase is part of a crystal-laden cold plume, it settles gravitationally or mixes with hot plumes originating at the boundary between the evolved host magma and the hotter more mafic magma (Couch et al., 2001). As a result, it will be partly resorbed and grow a new more calcic rim in the hotter environment. This plagioclase can then be transported up again within a hot plume generated at the bottom of the evolved upper layer of the magma system. In the cooler region crystals will again crystallize An-poor rims. Such a process would create abundant An contrasts and variable resorption morphologies. Since this mixing involves magmas of thermal but not compositional contrast, Fe content will remain relatively constant (Fig. 5a).

(2) The contrasting scenario for "compositional mixing" (Fig. 5b) is characterized by partial or complete homogenisation of two distinct magmas. In this case the calcium content will record the combined temperature, water *and* compositional effects, resulting in an increase in An. Fe and Mg in plagioclase will change according to changes in melt composition (Fig. 5b). This contrasting behaviour allows distinguishing between the compositional effect of thermal mixing and decompression versus compositional mixing, which we will explore in the following section.

5.4. Implications of An–Fe trends in El Misti plagioclase for the dynamics of the magmatic system

Applying the model developed above to the data presented in Fig. 3 reveals both, (a) a chemically closed-system evolution with only decompression and thermal effects and (b) the effects of open-system evolution with respect to temperature, water and composition. Plagioclase from sample MIS-02-102 (Fig. 3a–d) and MIS-99-10a/b (Fig. 6) shows steep An–Fe trends. This is accompanied by complexly zoned crystal populations and suggests compositional mixing as the major process

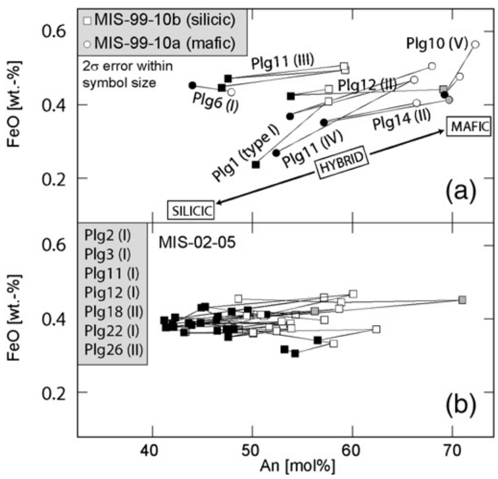

Fig. 6. a) An–Fe plot for mixed MIS-99-10a/b pumice samples. White, black and grey symbols refer to growth zones, resorption zones, and high An cores, respectively. Corresponding growth and resorption zones are connected to assess the steepness of An–Fe variations across a resorption interface. The numbers in parantheses refer to the different types of plagioclase observed in this sample. This sample with macro-scale heterogeneity records compositional mixing also on a microscale. Some plagioclase phenocrysts fall completely into scenario 2 of Fig. 5. Others may record a more hybrid stage of the magma. b) An–Fe plot for MIS-02-05. This sample is best characterized by scenario 1. Horizontal An–Fe trends characterize this sample.

during magma evolution of these rocks. In particular MIS-99-10a/b have a large variability in the An–Fe plot (Fig. 6) indicating that crystals have grown in both, evolved host, and more mafic hybrid magma. As expected, the mafic component (MIS-99-10a) is characterized by high An, high Fe concentrations with the exception of Plg6 that shows very low An concentrations at intermediate Fe levels. The silicic component (MIS-99-10b) has overall lower An and lower Fe concentrations. Not all crystals show steep correlations of An with Fe across a major resorption interface. Their moderately positive trends can also be caused by fO_2 variations; however in the light of the other An–Fe pattern in these samples and the textural mingling of two distinct magmas we prefer hybridization as mechanism for this sample. Thus, their intermediate An content and shallower An–Fe pattern are a result of reduced chemical and temperature contrasts due to ongoing hybridization. Two out of three phenocrysts (Plg 11, type IV; Plg1, type I) with steep pattern that show strong compositional mixing most likely resided in the silicic batch prior to mixing based on An–Fe systematics. Plg10 (type V) in the mafic end-member is probably a phenocryst of the mafic batch. MIS-99-10a/b demonstrated how a combination of hybridization and differentiation as well as thermal mixing and ascent can occur simultaneouosly, resulting in the stacked horizontal trends in An–Fe diagrams as demonstrated in the model (Fig. 5c) and observed in the data for the entire study (Fig. 7).

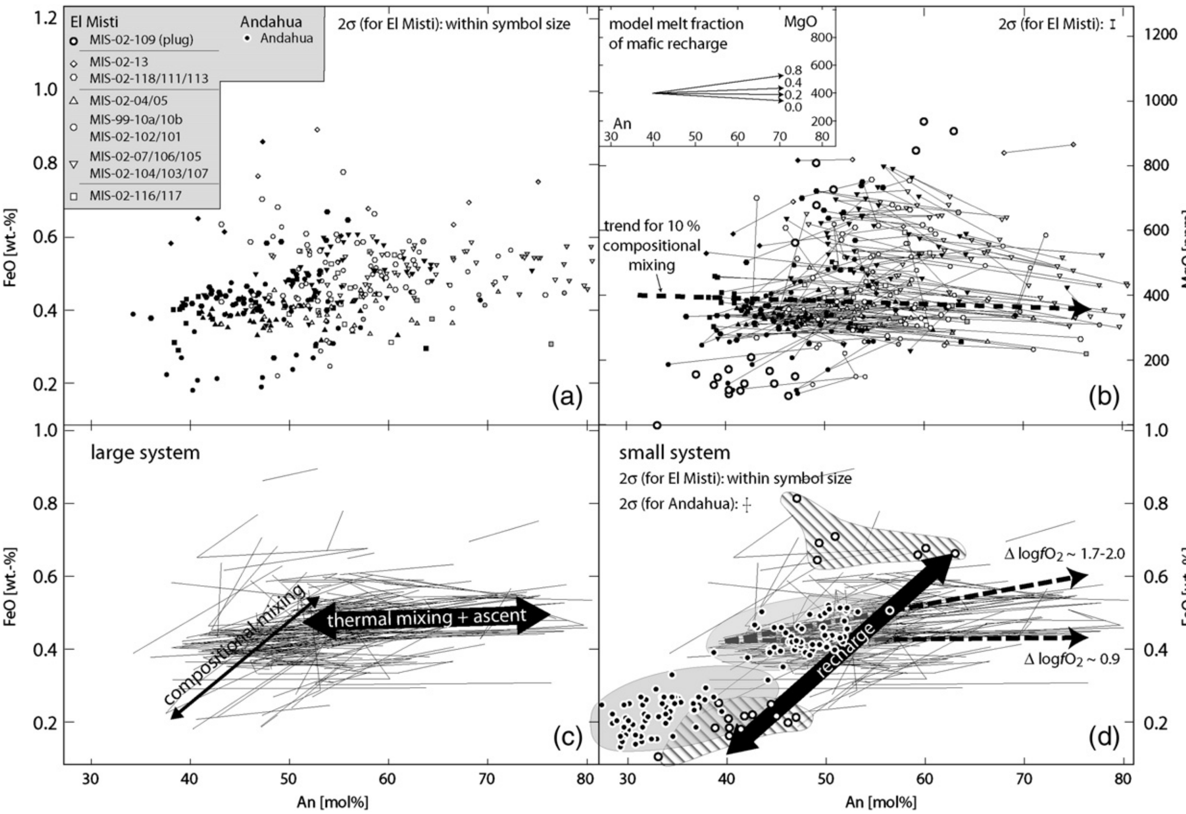

Fig. 7. a) An–Fe plot for the data of the large eruptions from El Misti volcano. White, black and grey color coding as in Fig. 6. Symbol shapes for samples of Fig. 6 have been changed to group samples with similar stratigraphic position and geochemical signature together. b) An–Mg plot. Corresponding growth and resorption zones are connected to display An–Mg variations across the resorption imterface. Dashed arrow is calculated as arrows in the inset: Model calculations for An–Mg behaviour associated with compositional mixing. Trends are more negative than the trend for 10% compositional mixing indicating that most samples show the closed-system evolution for An–Mg space. c) Connecting lines of growth and resorption zones for the An–Fe system. Data points were omitted for clarity. In general, the large El Misti magma system is dominated by flat An–Fe trends that are stacked at different Fe-levels. This indicates the dominance of closed-system behaviour (see text for further discussion). d) An–Fe plot for El Misti plug and AVF lavas. All samples represent volumetrically small eruptions. From core (low An, low Fe) to rim samples show a strong Fe enrichment, which is associated with a recharge event that triggered the eruption. The black lines represent the trends of data fields from Fig. 7c. Dashed arrows display An–Fe variations that are consistent with changes in oxygen fugacity, but no compositional mixing. The arrows correspond to the horizontal and slightly positive trends used for the oxygen fugacity assessment.

MIS-02-05 (Fig. 3e–i) shows no signs of mafic input and is mainly affected by thermal mixing and/or decompression (Figs. 5a, 6). The observed An–Fe variations across resorption events vary within the range that can be explained by changes in fO_2 as outlined in Section 5.2.

Feldspars from El Misti plug (MIS-02-109; Fig. 3k–n) and AVF record the most extreme examples for compositional mixing. It is important to note that they both represent small erupted volumes (Fig. 5b: scenario 2). Data cluster into two groups. Low-Fe homogeneous An-poor cores are overgrown by high-Fe An-rich rims as a result of compositional mixing and possibly decompression.

5.5. Large system vs. small system behaviour

The An–Fe systematics and the closed- vs. open-system behaviour will now be discussed separately for the large El Misti magma system and the small centers for the Andahua valley. The plug inside the historic crater is discussed together with the data of AVF since its eruptive volume is also very small and plagioclase zonation patterns are similar to those of Andahua lavas. Compiled Fe and Mg data for samples from El Misti reveal that most growth zones in the El Misti volcano data define subhorizontal An–Fe trends across major resorption interfaces as demonstrated for MIS-02-05 (Fig. 7a–c). According to Section 5.1 this indicates changes in temperature, pH_2O and oxygen fugacity but not in bulk composition. An–Mg trends are slightly negatively correlated, thus supporting the interpretation of limited compositional mixing (Fig. 7b). In fact, we can use the slopes of these trends in Fig. 7b and the partitioning relationship for Mg in plagioclase of Bindeman et al. (1998) to assess the role of compositional mixing for samples of El Misti. For a plagioclase of An40 containing 400 ppm MgO we calculate a intermediate liquid MgO content of 1.02 wt.%. Using the glass composition of MIS-02-104 as our best estimate for a typical El Misti mafic end-member we calculate an MgO content of 347 to 525 ppm in a plagioclase of An70 experiencing 0 to 80% compositional hypothetical mixing, respectively (insert in Fig. 7b). These calculations agree with limited compositional mixing as observed in the measured trends. Only 10 to 20% of mafic magma would strongly affect the slope of An–Mg trends, which is not observed in Fig. 7b.

The observed trends show stacks of horizontal lines (constant Fe, decreasing Mg with increasing An), which indicates that crystals record mostly closed-system evolution. However, the Fe-level of these horizontal trends varies considerable through time and between individual eruptive events. This suggests that replenishment through mafic recharge does in fact occur but remains cryptic and is not typically preserved in individual grains. Therefore, because mixing is not recorded by the phenocrysts, the typical time scale for recharge, mixing and complete homogenisation of the system is much larger than that of plagioclase crystallisation or it is not at all associated with plagioclase crystallisation. This is consistent with findings by Humphreys et al. (2006). Bindeman (1993) used mineral zonation patterns to estimate recharge volumes for volcanoes from the Kuriles–Kamchatka Arc. Typically for these examples the maximum recharge that intruded and actually mixed with a more differentiated resident magma in the reservoir does not exceed 10%.

If the volume of incorporated magma in fact represents the entire recharge volume, then such relatively small volumes may be easily accommodated in the main magma reservoir without immediate eruption. In particular, the accommodation is facilitated if the magma is water-oversaturated and contains compressible vesicles. Any cryptically mixed magma has to be less than 10% of the overall reservoir volume otherwise significant– and larger than observed– changes in the Mg content in plagioclase would be an expected consequence. This estimate is based on the composition of MIS-02-104, which is a typical mafic end-member at El Misti. More mafic end-members would require even smaller input volumes for mixing to remain cryptic in nature.

Singer et al. (1995) have seen similar closed-system behaviour for a single dacite flow at Volcan Tatara, which show constant An–Fe and decreasing An–Mg trends in plagioclase. They attribute this pattern to convective flow in a closed magma chamber to explain the observed Fe and Mg zonations. However, if this was the only process, it cannot explain such Fe–Mg–An zonations in plagioclase from lavas throughout the eruptive history of a mature stratovolcano. Therefore, some cryptic component of recharge and mixing is needed to keep the system thermally alive.

The small eruptive volumes represented by monogenetic centres of the Andahua valley and most recent El Misti plug clearly document different processes, because their plagioclases have steeply correlated An–Fe trends (Figs. 7d, 8, Table 2). fO_2 variations cannot explain such pattern since these would require changes of up to 5 log units in fO_2 (Table 2). In addition, An–Mg data for El Misti plug shows a pattern similar to An–Fe suggesting the Fe variations are independent of fO_2 (Fig. 7b). The uniformly steep An–Fe pattern within and– with few exceptions– between samples across

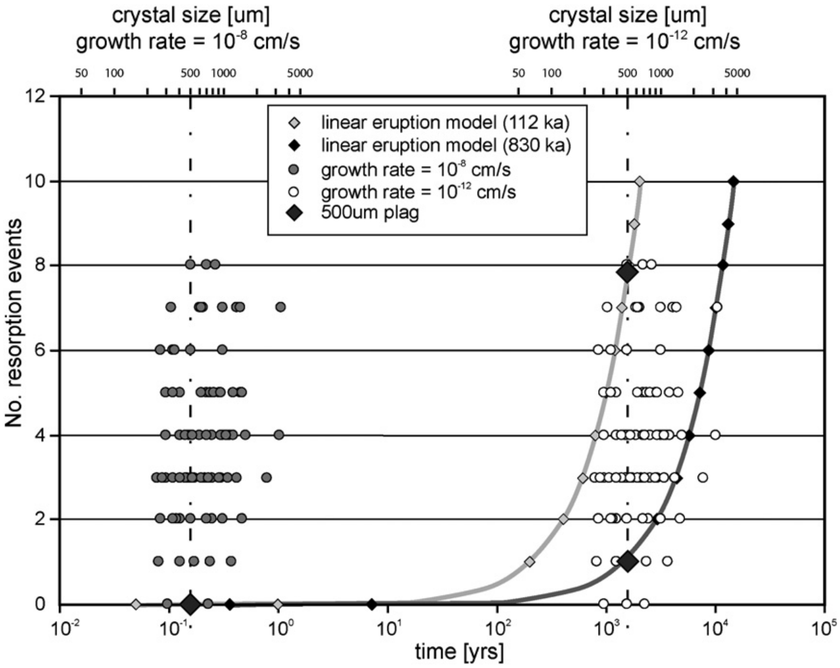

Fig. 8. Resorption events (resorption interfaces in El Misti plagioclase) vs. crystal residence time for two different growth rates (dark grey circles: 10^{-8} cm/s; white circles: 10^{-12} cm/s). Based on their crystal sizes, crystals are plotted at their corresponding residence time (see supplementary data). The linear eruption model has been calculated from the cone volume of El Misti and the estimated average volume of lava flows for El Misti ages of 112 ka (light grey diamonds) and 830 ka (dark grey diamonds). Based on this model a 500 µm model plagioclase (large triangles) should experience zero to eight resorption events in its residence time, assuming a growth rate of 10^{-8} and 10^{-12} cm/s, respectively.

only one major resorption zone are interpreted as being caused by a major recharge and compositional mixing event (Fig. 7d). Evidently, this recharge is also the triggering event for eruption since the rims are only10 to 20 µm wide. This suggests a time lag between mixing and eruption of only 1 day to 64 years based on a typical range of growth rates (Cashman, 1990; Davidson and Tepley, 1997). Similar time scales can be obtained from Mg diffusion time scales using the relation $x^2=Dt$. Here, D is the diffusion coefficient for Mg in plagioclase and x is the half width of the diffusional gradient (Costa et al., 2003). With a D of $3.5 \cdot 10^{-5}$ µm^2/s for An60 and, a typical temperature for El Misti of 950 °C (Legrende, 1999) we obtain for the time between rim crystallisation and eruption 8 days to 1 month. This estimate is similar to that based on the crystal growth rate.

Apparently, El Misti magmas are characterized by a high frequency of decompression and/or thermal and compositional mixing events, whereas the smaller Andahua magmatic system is affected only by one single recharge just prior to the eruption event. Thus the relative importance, frequencies and compositional contrasts of mixing are very different for these two types of systems. For the bulk of the El Misti eruption products, recharge and compositional mixing is apparently not a direct eruption trigger because each of the crystals shows a multitude of thermal mixing events in its history before they eventually erupted (Fig. 3). Based on growth rates and the number of resorption events per crystal, the importance of magma recharge as eruption trigger is now assessed (Fig. 8). The total number of thermal and cryptic mixing events and/or degassing episodes corresponds to the number of major resorption events. For a full documentation of all phenocrysts considered, see our supplementary data. Growth rates in volcanic systems are expected to be within 10^{-8} to 10^{-12} cm/s (Cashman, 1990; Davidson and Tepley, 1997). Minimum crystal ages were calculated for each plagioclase from their size and this range of growth rates.

While for fast growth rates crystal ages range from one month to one year, crystals in the slow case could have ages of 1000 to 10,000 years. Recent estimates of residence times for plagioclase crystals (Zellmer et al., 2003) suggest that shorter ages and thus faster growth rates may be more appropriate. This result can be compared with the average eruption frequency of El Misti. The eruption frequency was calculated by dividing the volume of El Misti cone through the volume of an average lava flow and the age of El Misti volcano. The age was taken to be 112 ka, which marks the onset of the main cone-building stage. The volume of around 80 km^3 is constrained by digital elevation models and field mapping. The average volume (0.145 km^3) for individual eruptions was estimated from a typical lava flow covering a sector of 20°, a run out of 5 km, and a typical thickness of 50 m. This linear eruption model is relatively robust compared to large uncertainties in growth rates and results in an eruption frequency of ~1/200 $years^{-1}$. Fig. 8 shows this eruption model with respect to the number of resorption events that should have occurred within a 500 μm model plagioclase for the two different growth rates.

The conclusions that can be taken from Fig. 8 for the large system are that for slow growth rates the eruption frequency equals the combined mixing/ascent frequency. For faster and more appropriate growth rates the eruption frequency is much smaller than the mixing frequency. Hence, at intermediate crystal growth rates phenocrysts survive on average several events of recharge, mixing and decompression before eventually being erupted. Davidson and Tepley (1997) also reported plagioclases from Chaos Crags (California), Purico-Chascon (Chile) and El Chichón (Mexico) that contain dissolution surfaces, which correspond to events occurring more frequently than actual eruptions. Therefore, mixing and step-wise decompression are the dominant mechanisms within the magma, but clearly not each mixing or decompression event must trigger an eruption from a large volcano. For the andesitic Volcan San Pedro (36 °S, Chilean Andes) Costa and Chakraborty (2004) also found multiple recharge events that did not lead to eruption. Such system behaviour is in particular true if crystal residence times are short (Zellmer et al., 2003) and if they record many resorption and therefore mixing and decompression events. Thus, in case of El Misti the observed magmatic pulses are mainly recorded as thermal disturbances or decompression events. This is consistent with extensive crystal dissolution within the host magma. Dissolution is most effective during slow recharge, where thermal and pH_2O equilibration can be obtained and armouring is minor, while chemical homogenisation and mixing is sluggish (Bindeman, 1993). Thus thermal mixing and ascent-stagnation events without immediate eruption may be the typical regime for a large magma system due to its volume buffering capacity. Chemical homogenisation between residing and recharge magma may then take place *between* the recharge and eruption events and may be of cryptic nature (Humphreys et al., 2006). This results in stacked flat An–Fe trends at different Fe levels.

6. How focussed is the El Misti magmatic system?

In Section 5 we have developed a model that is capable to explain the An–Fe signatures observed in plagioclase phenocrysts from El Misti. However, it is still unresolved whether the magma reservoir is represented by one single magma chamber or by an interconnected plexus of smaller reservoirs and dikes. Plagioclase heterogeneities can also be produced in small plumbing systems in which plagioclase populations of different batches are mixed. Such a mechanism may even be more suitable to juxtapose different populations as is typically observed in many samples. Hence, is a magma system with a series of contemporaneous small volume reservoirs not more likely beneath the volcano than one large magma reservoir?

There is currently no geophysical data of the appropriate scale at El Misti that could argue for a large magma chamber or a more complex plumbing system beneath the volcano. Nevertheless, there are several arguments in favour of a relatively large magma systems, which partly derive from considerations above. It is often argued that orogenic batholiths represent the magmatic systems beneath volcanic arcs (e.g. Sierra Nevada, California: Clemens-Knott and Saleeby, 1999; Coastal Batholith, Peru: Cobbing, 1982; Bussel and Pitcher, 1985). These systems extend over hundreds of kilometres and petrographic homogeneity can exceed more than ten kilometres (Bussell and Pitcher, 1985). Despite their compositional homogeneity, they probably represent many individual magma batches. In addition, Bussell and Pitcher (1985) report small individual intrusive volumes of a few km^3 within the Peruvian Coastal Batholith. Such volumes are appropriate for the El Misti magma system if the reservoir is only partially evacuated during any single eruption. Small scale compositional heterogeneities (less than 1 km) are rare in orogenic batholiths and thus larger volumes of magma reservoirs are indicated. Hence, field observations support the possibility that magmatic arc systems may be fed from single reservoirs at least several km^3 in volume. In addition to field constraints, thermal energy considerations favour the large continuous magma system. Small nested systems should solidify quite rapidly, while larger systems are able to maintain a liquid state over much longer timescales if intrusions are focussed spatially but distributed in time (Petford and Gallagher, 2001). Fe–An systematics also favour the existence of one main magma body. Mixing of different domains either derived from distinct batches or caused by variable physical and chemical conditions within a continuous reservoir is necessary to produce heterogeneous plagioclase populations. Mixing of chemically different magmas should result in a signature that would be recorded by Fe–An systematics in plagioclase crystals. Plagioclase An–Fe zonation of El Misti is consistent with a well-stirred system, in which intermittent homogenisation is attained. Thus, it is most likely that chemical variability persists in small systems while homogenisation will occur in larger systems.

Recharge and mixing, however, must also occur below El Misti to maintain the magmatic system active over >100 ka. A possible explanation is the “delayed entrainment” of recharge magma. In the first step this magma provides only heat to drive thermal mixing. During this stage the recharge magma will differentiate and reduces its chemical and physical contrast to the overlying residing magma. With time as density and compositional contrasts diminish compositional mixing of these two batches is more likely to occur. This process will first result mostly in thermal effects in the resident magma and magma recharge and mixing occurs cryptically.

During the early stages of El Misti the compositional variability within plagioclase phenocrysts was in fact larger than in younger products. This could be due to establishment of the main magma system by successive intrusions at this stage. Later products then would be better buffered thermally and compositionally than early magma batches. Only occasionally compositional heterogeneous batches, like MIS-99-10a/b, may be able to pass the compositional filter that usually homogenizes the magma system.

In addition, El Misti contains minor deposits of evolved compositions, such as the rhyolitic Chiguata Surge (Thouret et al., 2001). The most recent eruption of the plug in the present crater and the distinct zonation patterns of its phenocrysts also argue for the additional existence of small crystal-poor magma pockets. The production of such batches of crystal-poor melts can be explained by filter-pressing (Sisson and Bacon, 1999) or crystal compaction within a mush (Bachmann and Bergantz, 2004) that allows extracting high-silica melts from a high crystalline magma. Since both, the plug and the rhyolitic surge were erupted from the central crater, this observation suggests that small volumes may develop independently and can bypass or segregate from the large magma system. Whether or not this can happen depends on the longer-term temperature evolution of the system and could depend on the changing recharge rates with time.

7. Conclusions

We have investigated an extensive suite of volcanic rocks from El Misti volcano and the AVF. Samples cover the entire 112 kyrs of activity of El Misti volcano and in case of the AVF are representative for the monogenetic cinder cones in Andahua Valley. Our approach is based on plagioclase zonation patterns and trace element distributions within the plagioclase phenocrysts. Plagioclase phenocrysts of El Misti volcanics show large variations in their zonation patterns. Based on An–Fe we can distinguish between (a) “thermal mixing” (self-mixing) with a cryptical component of magma replenishment and (b) “compositional mixing”, in which chemically distinct batches mingle and hybridize. Compositional mixing characterizes the early stage of evolution (e.g. MIS-02-102). Samples from younger stratigraphic units representing the mature stage of stratocone building mostly show horizontal trends in An–Fe space. The system is chemically buffered by the large volume of resident magma. Only occasionally subordinate compositional mixing is present in younger samples.

The small El Misti plug and AVF monogenetic centres are very different in their plagioclase zonation patterns in having steep An–Fe correlations, which reflect compositional mixing. In these small systems, the mixing event always appears to have directly triggered the eruption.

Evidence presented here for a thermally maturing magma system has obvious implications for assessing the conditions within reservoirs feeding large stratovolcanoes and the hazard assessment of such systems.

Recharge events are *not* the dominant trigger for volcanic eruption for the large system. The frequency of resorption events and crystal growth rates reveals that mixing (both thermal and chemical) as well as decompression-stagnation episodes occur more frequently in the system than eruptions. For fast crystal growth rates, which are more consistent with evidence for short residence times, plagioclase crystals record many mixing events. This indicates that the time scale of crystallisation is much longer than the time scale of mixing and decompression within the magma system. Crystals thus “survive” many mixing, decompression, recharge and eruption events before they are eventually erupted. If mixing and/or decompression occurs more frequently than eruptions, then recharge cannot be the (only) eruption trigger. Whereas the common presence of mafic enclaves have been cited as arguments for magma mingling triggering eruptions, our detailed studies now demonstrate that mixing may be far more frequent than eruptions. This casts some doubt on magma mixing as the “standard” eruption trigger for large mature stratovolcanoes. Several other parameters may play a role that determine whether or not recharge leads to eruption: (1) recharge volume, (2) recharge volatile content, (3) recharge rate.

Acknowledgements

We would like to thank Jean-Claude Thouret for helpful discussions and invaluable support in the field, Gerald Hartmann for XRF analyses, Andreas Kronz for skillful assistance with the microprobe analyses as well as Joe Dufek and Kari Cooper for insightful comments on an earlier version of the manuscript. This work was funded by the DFG project WO 362/18 (GW). Reviews by Fidel Costa and Anita Grunder have substantially improved this manuscript. Audrey Martin was involved at an early stage of this study and helped with the analyses of Andahua samples.

Appendix A. Supplementary data

Supplementary data associated with this article can be found, in the online version, at doi:10.1016/j.jvolgeores.2007.06.002.

References

Bachmann, O., Bergantz, G.W., 2004. On the origin of crystal-poor rhyolites: extracted from batholithic crystal mushes. Journal of Petrology 45 (8), 1565–1582.

Behrens, H., Johannes, W., Schmalzried, H., 1990. On the mechanisms of cation diffusion processes in Ternary feldspars. Physics and Chemistry of Minerals 17, 62–78.

Bergantz, G.W., Breidenthal, R.E., 2001. Non-stationary entrainment and tunnelling eruptions: a dynamic link between eruption processes and magma mixing. Geophysical Research Letters 28, 3075–3078.

Bindeman, I.N., 1993. A practical petrological method for the determination of volume proportions of magma chamber refilling. Journal of Volcanology and Geothermal Research 56, 133–144.

Bindeman, I.N., Davis, A.M., Drake, M.J., 1998. Ion microprobe study of plagioclase-basalt partition experiments at natural concentration levels of trace elements. Geochimica et Cosmochimica Acta 62, 1175–1193.

Blundy, J., Wood, B., 1994. Prediction of crystal-melt partition coefficients from elastic moduli. Nature 372, 452–454.

Blundy, J., Cashman, K., Humphreys, M., 2006. Magma heating by decompression-driven crystallization beneath andesite volcanoes. Nature 443, 76–80.

Brown, W.L., Parsons, I., 1994. Feldspars in igneous rocks. In: Parsons, I. (Ed.), Feldspars and Their Reactions. NATO ASI Series C, vol. 421, pp. 449–499.

Burnham, C.W., 1994. Development of the Burnham model for prediction of H_2O solubility in magmas. In: Carrol, M.C., Holloway, J.R. (Eds.), Volatiles in Magmas. Reviews in Mineralogy, vol. 30, pp. 123–129.

Bussell, M.A., Pitcher, W.S., 1985. The structural controls of batholith emplacement. In: Pitcher, W.S., Atherton, M.P., Cobbing, E.J., Beckinsale, R.D. (Eds.), Magmatism at a Plate Edge: The Peruvian Andes. Blackie, London, pp. 167–176.

Cashman, K.V., 1990. Textural constraints on the kinetics of crystallization of igneous rocks. In: Nicholls, J., Russell, J.K. (Eds.), Modern Methods of Igneous Petrology, Understanding Magmatic Processes. Mineralogical Society of America, Reviews in Mineralogy, vol. 24, pp. 259–314.

Clemens-Knott, D., Saleeby, J.B., 1999. Impinging ring dike complexes in the Sierra Nevada Batholith, California; roots of the Early Cretaceous volcanic arc. Geological Society of America Bulletin 111, 484–496.

Cobbing, E.J., 1982. The segmented Coastal Batholith of Peru: its relationship to volcanicity and metallogenesis. Earth Science Reviews 18, 241–251.

Costa, F., Chakraborty, S., 2004. Decadal time gaps between mafic intrusion and silicic eruption obtained from chemical zoning patterns in olivine. Earth and Planetary Science Letters 227, 517–530.

Costa, F., Chakraborty, S., Dohmen, R., 2003. Diffusion coupling between trace and major elements and a model for calculation of magma residence times using plagioclase. Geochimica et Cosmochimica Acta 67, 2189–2200.

Couch, S., Sparks, R.S.J., Carroll, M.R., 2001. Mineral disequilibrium in lavas explained by convective self-mixing in open magma chambers. Nature 411, 1037–1039.

Davidson, J.P., Tepley III, F.J., 1997. Recharge in volcanic systems: evidence from isotope profiles of phenocrysts. Science 275, 826–829.

Delacour, A., Gerbe, M.C., Thouret, J.C., Wörner, G., Paquereau-Lebti, P., 2007. Magma evolution of Quaternary minor volcanic centers in Southern Peru, Central Andes. Bulletin of Volcanology 69, 581–608.

de Silva, S.L., Francis, P.W., 1991. Volcanoes of the Central Andes. Springer-Verlag, New York. 216 pp.

Ginibre, C., Kronz, A., Wörner, G., 2002a. High-resolution quantitative imaging of plagioclase composition using accumulated backscattered electron images: new constraints on oscillatory zoning. Contributions to Mineralogy and Petrology 142, 436–448.

Ginibre, C., Wörner, G., Kronz, A., 2002b. Minor- and trace-element zoning in plagioclase: implications for magma chamber processes at Parinacota Volcano, northern Chile. Contributions to Mineralogy and Petrology 143, 300–315.

Hammer, J., Rutherford, M., 2002. An experimental study of the kinetics of decompression-induced crystallization in silicic melt. Journal of Geophysical Research 107 (B1), 2021.

Holloway, J.R., Blank, J.G., 1994. Application of experimental results to C–O–H species in natural melts. In: Carrol, M.C., Holloway, J.R. (Eds.), Volatiles in Magmas. Reviews in Mineralogy, vol. 30, pp. 187–230.

Housh, T.B., Luhr, J.F., 1991. Plagioclase-melt equilibria in hydrous systems. American Mineralogist 76, 477–492.

Humphreys, M.C.S., Blundy, J.D., Sparks, R.S.J., 2006. Magma evolution and open-system processes at Shiveluch volcano: insights from phenocryst zoning. Journal of Petrology 47, 2303–2334.

Jaupart, C., Tait, S., 1995. Dynamics of differentiation in magma reservoirs. Journal of Geophysical Research 100, 17615–17636.

Knesel, K.M., Davidson, J.P., Duffield, W.A., 1999. Evolution of silicic magma through assimilation and subsequent recharge: evidence from Sr isotopes in Sanidine phenocrysts, Taylor Creek Rhyolite, NM. Journal of Petrology 40 (5), 773–786.

Legrende C., 1999. Pétrogenese du volcan “Misti moderne” (Sud Pérou): essai de caractérisation de l’évolution pétro-géochimique et chronologique. DEA thesis, Université Blaise-Pascal, Clermont-Ferrand. 82 pp.

Marsh, B.D., 1988. Crystal capture, sorting, and retention in convecting magma. Geological Society of America Bulletin 100, 1720–1737.

Marsh, B.D., 1989. On convective style and vigor in sheet-like magma chambers. Journal of Petrology 30, 479–530.

Nelson, S.T., Montana, A., 1992. Sieve-textured plagioclase in volcanic-rocks produced by rapid decompression. American Mineralogist 77 (11–12), 1242–1249.

Paquereau-Lebti, P., Thouret, J.C., Wörner, G., Fornari, M., 2006. Neogene and Quaternary ignimbrites in the area of Arequipa, Southern Peru: stratigraphical and petrological correlations. Journal of Volcanology and Geothermal Research 154, 251–275.

Petford, N., Gallagher, K., 2001. Partial melting of mafic (amphibolitic) lower crust by periodic influx of basaltic magma. Earth and Planetary Science Letters 193, 483–499.

Rutherford, M.J., Hill, P.M., 1993. Magma ascent rates from amphibole breakdown: an experimental study applied to the 1980–1986 Mount St. Helens eruptions. Journal of Geophysical Research 98 (B11), 19667–19685.

Singer, B.S., Dungan, M.A., Layne, G.D., 1995. Textures and Sr, Ba, Mg, Fe, K, and Ti compositional profiles in volcanic plagioclase: clues to the dynamics of calc-alkaline magma chambers. American Mineralogist 80, 776–798.

Snyder, D., Tait, S., 1996. Magma mixing by convective entrainment. Nature 379, 529–531.

Sisson, T.W., Bacon, C.R., 1999. Gas-driven filter pressing in magmas. Geology 27, 613–616.

Sugawara, T., 2000. Thermodynamic analysis of Fe and Mg partitioning between plagioclase and silicate liquid. Contributions to Mineralogy and Petrology 138, 101–113.

Sugawara, T., 2001. Ferric iron partitioning between plagioclase and silicate liquid: thermodynamics and petrological applications. Contributions to Mineralogy and Petrology 141, 659–686.

Thouret, J.C., Finizola, A., Fornari, M., Legeley-Padovani, A., Suni, J., Frechen, M., 2001. Geology of El Misti volcano near the city of Arequipa, Peru. GSA Bulletin 113 (12), 1593–1610.

Tomiya, A., Takahashi, E., 2005. Evolution of the magma chamber beneath Usu volcano since 1663: a natural laboratory for observing changing phenocryst compositions and textures. Journal of Petrology 46 (12), 2395–2426.

Triebold, S., Wörner, G., Kronz, A., 2006. Anorthite- and celsian-calibrated backscattered electron profiles, trace elements, and growth textures in feldspars from the Teide-Pico Viejo volcanic complex (Tenerife). Journal of Volcanology and Geothermal Research 154, 117–130.

Wallace, G.S., Bergantz, G.W., 2005. Reconciling heterogeneity in crystal zoning data: an application of shared characteristic diagrams at Chaos Crags, Lassen Volcanic Center, California. Contributions to Mineralogy and Petrology 149, 98–112.

Wilke, M., Behrens, H., 1999. The dependence of partitioning of iron and europium between plagioclase and hydrous tonalitic melt on oxygen fugacity. Contributions to Mineralogy and Petrology 137, 102–114.

Zellmer, G.F., Sparks, R.S.J., Hawkesworth, C.J., Wiedenbeck, M., 2003. Magma emplacement and remobilization timescales beneath Montserrat: insights from Sr and Ba zonation in plagioclase phenocrysts. Journal of Petrology 44 (8), 1413–1431.